Check for updates

Article

The International Journal of Robotics Research
2021, Vol. 40(4-5) 747–763
© The Author(s) 2021
Article reuse guidelines:
sagepub.com/journals-permissions
DOI: 10.1177/0278364921991158
journals.sagepub.com/home/ijr
SAGE

Coordination of lateral body bending and leg movements for sprawled posture quadrupedal locomotion

Baxi Chong[1], Yasemin Ozkan Aydin[1], Chaohui Gong[2], Guillaume Sartoretti[3], Yunjin Wu[3], Jennifer M Rieser[1], Haosen Xing[3], Perrin E Schiebel[1], Jeffery W. Rankin[4], Krijn B Michel[5], Alfredo Nicieza[6], John R Hutchinson[5], Daniel I Goldman[1] and Howie Choset[3]

Abstract

Many animals generate propulsive forces by coordinating legs, which contact and push against the surroundings, with bending of the body, which can only indirectly influence these forces. Such body–leg coordination is not commonly employed in quadrupedal robotic systems. To elucidate the role of back bending during quadrupedal locomotion, we study a model system: the salamander, a sprawled-posture quadruped that uses lateral bending of the elongate back in conjunction with stepping of the limbs during locomotion. We develop a geometric approach that yields a low-dimensional representation of the body and limb contributions to the locomotor performance quantified by stride displacement. For systems where the damping forces dominate inertial forces, our approach offers insight into appropriate coordination patterns, and improves the computational efficiency of optimization techniques. In particular, we demonstrate effect of the lateral undulation coordinated with leg movement in the forward, rotational, and lateral directions of the robot motion. We validate the theoretical results using numerical simulations, and then successfully test these approaches using robophysical experiments on granular media, a model deformable, frictional substrate. Although our focus lies primarily on robotics, we also demonstrate that our tools can accurately predict optimal body bending of a living salamander Salamandra salamandra.

Keywords

Bio-inspired robot, legged locomotion, geometric mechanics

1. Introduction and summary

Animals, and increasingly robots, can use limbs to propel themselves to maneuver across a variety of terrains (Buehler et al., 1998; Kolter et al., 2008; McGhee and Iswandhi, 1979; Saranli et al., 2001; Zucker et al., 2011). In addition to these appendages, undulatory body motions can also contribute to locomotor propulsion, even when not directly in contact with the environment. For example, salamanders (Crespi et al., 2013; Daan and Belterman, 1968; Frolich and Biewener, 1994; Roos, 1964), lizards (Farley and Ko, 1997), and some mammals (Kafkafi and Golani, 1998) use lateral body undulation in coordination with their legs for effective locomotion. While previous studies have elucidated the benefits of using lateral body undulation in conjunction with quadrupedal limb motion for individual tasks such as walking, running, or turning (Crespi et al., 2013; Daan and Belterman, 1968; Kafkafi and Golani, 1998; Roos, 1964), no general framework yet exists to systematically explore coordination and performance in quadrupedal systems that employ body undulatory motion, or more specifically back bending. Building this framework is challenging because it requires not only coordinating many degrees of freedom (DoFs), but also coordinating different types of DoFs (i.e., body bending

[1]Georgia Institute of Technology, Atlanta, GA, USA
[2]BITO Robotics, Inc., Pittsburgh, PA, USA
[3]Carnegie Mellon University, Pittsburgh, PA, USA
[4]Rancho Research Institute, Downey, CA, USA
[5]Royal Veterinary College, London, UK
[6]University of Oviedo, Oviedo, Spain

Corresponding author:
Baxi Chong, Complex Rheology And Biomechanics Laboratory, Howey Physics Building, 837 State Street NW, Atlanta, GA 30332, USA.
Email: bchong9@gatech.edu

and the leg movements) in different types of behaviors (i.e., forward, turning, and sideways motion).

Since the 1980s, a framework referred to as "geometric mechanics" has been developed (Batterman, 2003; Kelly and Murray, 1995; Marsden, 1997; Ostrowski and Burdick, 1998; Shammas et al., 2007; Shapere and Wilczek, 1989; Wilczek and Shapere, 1989) as a general scheme to link locomotor performance to arbitrary patterns of "self-deformation." This scheme replaces laborious calculation with a geometric approach to gain qualitative and quantitative insight into how animal and robots can generate optimal high-level control (Astley et al., 2020; Full and Koditschek, 1999) to affect desired behaviors, such as forward, sideways, or turning locomotion.

In the geometric mechanics framework, the motion of a self-propelling system is separated into a shape space (the internal joint angle space) and a position space (position and orientation of locomotor in the world frame). The relationship between velocities in a shape space (joint angle velocities) and velocities in a position space (body velocities of the robot) is called the local form of the *connection*. A *gait* then maps a periodic path in the shape space to a displacement in the position space. One of the advantages of this approach is that it can readily generate, as well as evaluate, the displacement of gaits; this generative tool is based on a *height function* (sometimes called a connection vector field) which is essentially the curl of the connection (Gong et al., 2016, 2018; Hatton et al., 2013). In the last decade, our group has successfully advanced this scheme to enable gait design for limbless undulatory swimming systems in highly damped situations such as granular media, where the full contact between the system and the environment is maintained (Dai et al., 2016; Gong et al., 2016; Hatton et al., 2013). Importantly, the theoretical predictions have quantitative agreement with the experimental measurements, demonstrating that the geometric mechanics framework can be successfully applied to real-world systems.

Here we expand the scope of geometric mechanics to four-legged body-bending systems. The challenges of extending geometric mechanics to quadrupedal systems lie in the fact that these systems periodically make and break contact with the environment. In this article, we prescribe the leg contact states by their phase; this phase, together with the body-bending angle, forms the shape space, in which we can apply geometric mechanics tools. We demonstrate that proper body undulation, obtained from optimization in the new shape space, can improve the locomotion performance of our quadrupedal robots in forward, rotational and lateral directions. Furthermore, experimental data collected from fire salamanders (*Salamandra salamandra*) (Figure 1(a)) reveal that our geometric-based approach closely predicts motion observed in a biological system. The article is structured as follows: Section 2 provides an overview of related work; Section 3 introduces geometric mechanics and its extension to cylindrical shape spaces; Section 4 presents analytical results of our designed gaits;

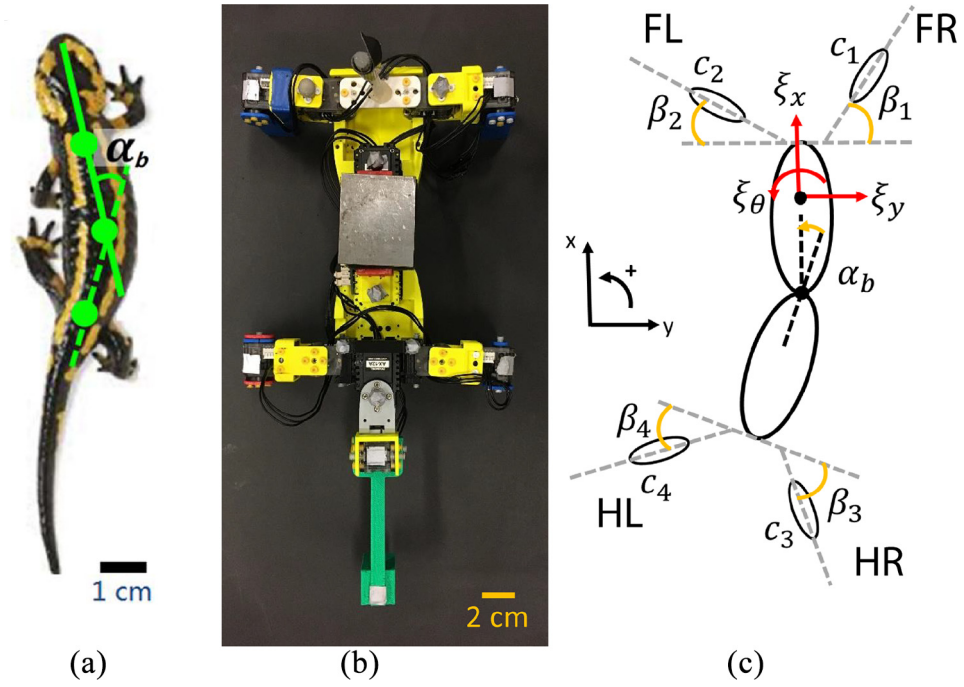

Fig. 1. The animal, robot, and theoretical models studied in this article. (a) Top view of a fire salamander. The body angle, α_b, is defined as an angle between the center lines that are parallel to the front and the back part of the body. (b) Top view of the robophysical model. It has two body parts connected with a servo, four 2-DoF legs, and a tail. The metal part at the center is used to pick up the robot with an electromagnetic gripper. All legs and tail have the same foot geometry (24×24 mm^2 cube shape). (c) The theoretical model with shape variables and body velocities labeled.

Section 5 presents experimental results of our designed gaits; finally, we discuss the role of lateral body undulation during quadrupedal locomotion in Section 6.

2. Related work

2.1. Leg movement

There has been extensive research showing that the design of appropriate leg movements can enable effective robot movement in a variety of environments (Buchli et al., 2009; Buehler et al., 1998; Cham et al., 2004; Kalakrishnan et al., 2011; Kolter et al., 2008; McGhee and Iswandhi, 1979; Saranli et al., 2001; Zucker et al., 2011). These approaches tend to be classified into one of several categories, including planning for appropriate foot contacts to maintain static stability during each phase of the step (Buchli et al., 2009; Kalakrishnan et al., 2011; Kolter et al., 2008; McGhee and Iswandhi, 1979; Zucker et al., 2011), or relying on dynamical stability by creating an appropriate robot morphology (for example, robot with six springy legs) (Buehler et al., 1998; Cham et al., 2004; Saranli et al., 2001).

One of the most popular approaches is to plan for foot contacts to ensure stability of feet and body. Foot placement determines a sequence of locations on the ground where a system places the distal-most portion of its limbs. Foot placement techniques may optimize criteria like stability and redundancy when applied to multi-legged locomotion. McGhee and Iswandhi (1979) introduced a heuristic gait-planning algorithm for legged robots by maximizing stability margin (the distance from the center of mass to the supporting polygon in the direction of travel) and minimizing kinematic margin (the distance that the foothold of a given leg can travel in the opposite direction of motion before reaching the boundary of its workspace). Although this algorithm was adequate for hexapods, it is not as well suited to quadrupeds because quadrupeds have more strict stability criteria. Bai et al. (1999) applied a similar approach to quadrupeds, which took a lateral sequence walk (leg lifting follows the sequence: left hind leg, left front leg, right hind leg, right front leg (Hildebrand, 1965)) as a primary gait and successfully adapted it to the environment. These ideas were applied to the Little Dog platform (Kolter et al., 2008; Zucker et al., 2011), where the footsteps are planned and implemented across rough terrain in the presence of disturbances.

More recently, machine learning tools and algorithms have been applied to design leg movements during locomotion. Kim and Uther (2003) applied Powell's minimization method (Powell, 1964) to design a periodic footfall pattern for quadrupedal robots that was faster and more stable than previous hand-optimized gaits in the RoboCup soccer competition. Kohl and Stone (2004) parameterized leg movements based on *locus* feet trajectory (Stone et al., 2003), then optimized these parameters to improve locomotion speed by a policy gradient method. With improved physical simulator and learning robust policies, Tan et al. (2018) trained the robot control policy in simulation and successfully implemented trotting and galloping gaits on agile quadrupedal robots.

Leg movement design has also been influenced by the study of biological systems: another approach relies less on rapid closed-loop control for foot placement and instead leverages appropriately tuned mechanics to achieve rapid dynamically and statically stable locomotion over diverse substrates. Inspired by cockroaches racing over a rough surface, Saranli et al. (2001) showed that RHex, a hexapod robot (Altendorfer et al., 2001; Buehler et al., 1998, 1999), exhibited the ability for forward locomotion in uneven terrain and in the presence of obstacles.

Of specific interest to this work, Nyakatura et al. (2019) used a combination of experimental studies with living animals, a robophysical model, and kinematic plus dynamic simulations to test how animals with more sprawled postures moved, in order to infer how an extinct animal *Orobates pabsti* might have conducted quasi-steady forward walking locomotion. Their "sprawling gait space" approach is also complementary to ours, showing how the parameters of body undulation, body height ("sprawledness"), long-axis rotation of the proximal leg joints, and leg retraction motion help describe locomotor differences between four extant species and *Orobates*.

2.2. CPG-based approach

Inspired by analogous ideas from biology, the central pattern generator (CPG) approach uses periodic signals to drive body joint trajectories in shape space for locomotion or other repetitive tasks (Holmes et al., 2006; Ijspeert, 2020; Nyakatura et al., 2019; Rossignol et al., 2006; Suzuki et al., 2019) to augment the performance of an existing footfall pattern. Ijspeert et al. (2007) showed that CPGs can produce body–limb coordinated movements for the locomotion of a salamander robot, as well as generate gait transitions among different forward gait motions of varying speeds. Using CPG analytic tools, Crespi et al. (2013), Horvat et al. (2017), and Eckert et al. (2015) demonstrated that the body–limb coordination used by salamanders optimizes their forward speed and produce turning motion. Following this idea, Owaki et al. (2013) investigated the mechanisms of inter-limb coordination which exhibit good adaptability to changes in walking speed of a quadrupedal robot.

Some recent CPG work has included body bending in robot motion design (Crespi et al., 2013; Cruse, 1990; Horvat et al., 2017; Ijspeert et al., 2007; Owaki et al., 2013)). In contrast to the feedback control algorithms in CPGs, our gait design algorithms do not require prior knowledge of gait formula. Indeed, our approach can be used as an input for CPG-based approaches. That is, our gait design process can be used to generate and optimize gait trajectories, which can then be tracked online by a set of coupled oscillators.

2.3. Turning motion

Turning motions in quadrupedal robots have been less studied. In addition, existing turning policies of quadrupedal robots heavily rely on leg placement: previous work has shown that careful foot placement planning can enable quadrupedal turning motions (Bien et al., 1991). Cho et al. (1995) introduced the footfall planning objective function, where speed, stability, translation direction, and turning were all included. Palmer and Orin (2006) designed a turning fuzzy controller by placing the fore legs to the outside of the turn and the hind legs to the inside. In addition to the control algorithms in foot placement, biologists indicate that body bending also plays an important role during turning motion. For example, Kafkafi and Golani (1998) showed the body shape changed from *S*-shape to *C*-shape during the turning motion of ferrets.

Legs movements and body undulations can both lead to quadrupedal turning motions. In this article, we investigate how leg movement modulation can coordinate with body undulation to enable different turning behaviors in quadrupedal locomotion from in-place turning to steering.

3. Geometric approach to gait design

The geometric approach, which we use to study the body–leg coordination during quadrupedal locomotion, develops systematic tools which can generate open-loop templates for gaits which can lead to locomotor motion of desired capacities. Before we discuss our improvements, we provide an overview of geometric mechanics and then extend geometric mechanics tools to legged systems. We use resistive force theory (RFT) to model the ground reaction forces (GRFs) between our robots and granular environments (Zhang and Goldman, 2014). Recent work (Astley et al., 2020) revealed this approach to be effective on frictional ground as well.

3.1. Geometric mechanics overview

Geometric mechanics techniques typically separate the system's configuration space into a position space and a shape space. The position space denotes the location of the system relative to a world frame, and the shape space denotes the range of internal configuration (the shape) of the system. Geometric mechanics techniques then seek to establish a relationship between the velocities of these spaces; this relationship is often called a *connection* and it shares many properties with a robot manipulator's Jacobian. In this section, we provide a concise overview of the geometric tools needed for this article, but for a more detailed and comprehensive review, we refer readers to Kelly and Murray (1995), Ostrowski and Burdick (1998), Shapere andWilczek (1989),Wilczek and Shapere (1989), Bloch et al. (1996), Marsden and Ratiu (2013), Batterman (2003), Hatton and Choset (2015), and Gong et al. (2018).

3.1.1. Kinematic reconstruction equation. In principally kinematic systems, where the damping (frictional) forces dominate the inertial force, the equation of motion of a system operating in the plane with two internal DoFs reduce to

$$\boldsymbol{\xi} = \boldsymbol{A}(\boldsymbol{r})\dot{\boldsymbol{r}} \tag{1}$$

where $\boldsymbol{\xi} = [\xi_x\ \xi_y\ \xi_\theta]^{\mathrm{T}}$ denotes the body velocity in forward, lateral, and rotational directions, respectively (position variable); $\boldsymbol{r} = [r_1\ r_2]^{\mathrm{T}}$ denotes the two-dimensional shape variable; and $\boldsymbol{A}(\boldsymbol{r})$ is the local connection matrix that relates shape velocity $\dot{\boldsymbol{r}}$ to body velocity $\boldsymbol{\xi}$. Equation (1) is also called the *kinematic reconstruction equation* (Hatton and Choset, 2015; Hatton et al., 2013; Murray et al., 1994).

3.1.2. Connection vector fields and height functions. Each row of the local connection matrix $\boldsymbol{A}(\boldsymbol{r})$ corresponds to a component direction of the body velocity and therefore gives rise to a connection vector field (Figure 2(a)). The body velocities in the forward, lateral and rotational directions are respectively computed as the dot product between connection vector fields and the shape velocity $\dot{\boldsymbol{r}}$.[1] A shape velocity $\dot{\boldsymbol{r}}$ along the direction of the vector field would yield the largest possible body velocity in that direction, whereas a shape velocity $\dot{\boldsymbol{r}}$ orthogonal to the field would produce zero body velocity.

A *gait* is represented as a path in the shape space that begins and ends at the same point. Figure 2(a) shows a typical vector field for limbless locomotion in an Euclidean shape space, where gaits appear as closed loops. The displacement along the gait path $\partial\phi$ can be obtained by integrating the ordinary differential equation (Hatton and Choset, 2015)

$$g(T) = \int_{\partial\phi} T_e L_{g(\boldsymbol{r})} \boldsymbol{A}(\boldsymbol{r}) d\boldsymbol{r} \tag{2}$$

where $g(t) = [x(t), y(t), \alpha(t)]^{\mathrm{T}} \in SE(2)$ represents the position and rotation of body frame viewed in the worlds frame (Murray et al., 1994); $g(T) = [\Delta x, \Delta y, \Delta\alpha]^{\mathrm{T}}$ denotes the translation and rotation of the body frame (with respect to the world frame) in one gait cycle. Note that $T_e L_g$ is the left-lifted action with respect to the coordinates of g:

$$T_e L_g = \begin{bmatrix} \cos(\alpha) & -\sin(\alpha) & 0 \\ \sin(\alpha) & \cos(\alpha) & 0 \\ 0 & 0 & 1 \end{bmatrix} \tag{3}$$

Note that the integral of (2) can be approximated to the first order by

$$\begin{pmatrix} \Delta x \\ \Delta y \\ \Delta\alpha \end{pmatrix} = \int_{\partial\phi} \boldsymbol{A}(\boldsymbol{r}) d\boldsymbol{r} \tag{4}$$

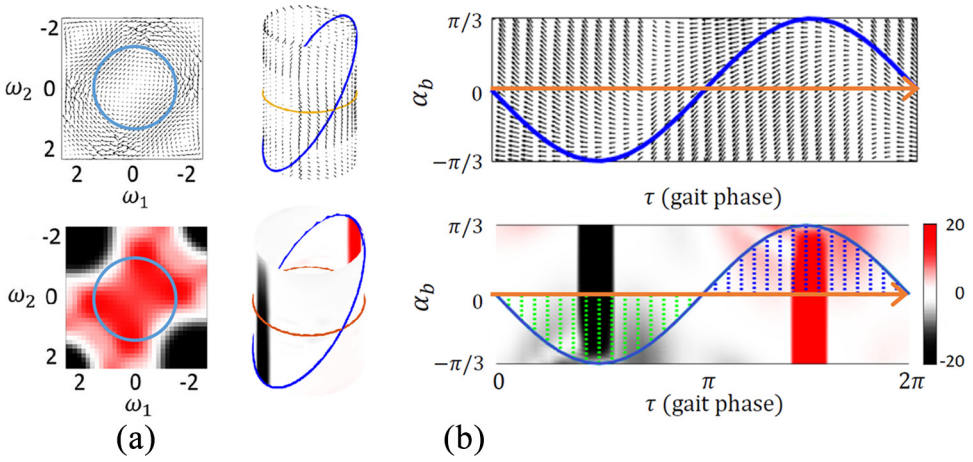

Fig. 2. The connection vector field and the height functions in the reduced shape space for two different systems. (a) The connection vector field (top) and the height function (bottom) in an Euclidean shape space corresponding to motions in the forward direction of a 3-link snake robot (w_1 and w_2 denote the body joints) slithering on the surface of ~1 mm poppy seeds. The blue circle represents a gait path in the corresponding shape space. (b) The connection vector field (top) and the height function (bottom) in a cylindrical shape space corresponding to the forward motion of a quadruped robot moving with a four-beat walking gait on the surface of ~1 mm poppy seeds. We show the vector field and height function on a cylindrical space and on the Euclidean parameterization of a cylindrical space. The blue curve represents a sample gait in the corresponding cylindrical shape space. Orange lines represent the assistive lines to form closed loops with the gait path in the unfolded cylindrical shape space. The area in the blue shading represents the area where the gait path and the assistive line form a clockwise loop; the area in the green shading represents the area where the gait path and the assistive line form a counterclockwise loop. Red, white, and black colors indicate positive, zero, and negative values in the height function, respectively.

According to Stokes' theorem, the path integral along a closed curve $\partial\phi$ is equal to the surface integral of the curl of $\boldsymbol{A}(\boldsymbol{r})$ over the area enclosed by $\partial\phi$:

$$\int_{\partial\phi} \boldsymbol{A}(\boldsymbol{r})d\boldsymbol{r} = \iint_{\phi} \nabla \times \boldsymbol{A}(\boldsymbol{r})d\boldsymbol{r}_1 d\boldsymbol{r}_2 \tag{5}$$

ϕ denotes the area enclosed by a gait path $\partial\phi$. The curl of the connection vector field $\nabla \times \boldsymbol{A}(\boldsymbol{r})$ is referred to as the height function (Figure 2(a)). The three rows of the local connection matrix $\boldsymbol{A}(\boldsymbol{r})$ can thus produce three height functions, which we call the *forward height function*, $\boldsymbol{H_x}$, the *lateral height function*, $\boldsymbol{H_y}$, and the *rotational height function*, $\boldsymbol{H_\theta}$.

With the above derivation (1), (4), and (5), we simplify the gait design for limbless locomotion to drawing a closed loop in an Euclidean shape space. The displacements are approximated by the surface integral over area on the height function enclosed by the gait path. For example, in Figure 2(a), drawing the circle with the most surface integral represents designing the circular gait with the largest forward displacement.

3.1.3. Periodic shape spaces. Often, a shape space can have a periodic structure. As in the case for the legged systems examined in this article, we introduced a (cyclic) phase variable to prescribe the contact patterns. Most prior work only applied geometric mechanics to Euclidean shape space. In this article, we formulate the body undulatory quadrupedal locomotion as gait design on a two-dimensional cylindrical shape space (Figure 2(b)), where one axis (α_b) represents the body bending angle and the other axis (τ) represents the phase of *all* of the leg movements. In doing so, we are able to extend geometric mechanics to study legged systems.

To form an enclosed area in the Euclidean parameterization of the periodic shape space, we introduce the notion of an assistive line (Gong et al., 2018). The assistive line is defined to be a path in shape space where only one shape variable changes and is used to form a closed loop with the gait path in the shape space. Note that, in principle, the choice of assistive line is arbitrary with respect to the same winding number. In practice, we often choose the assitive line with a physical meaning. In this example, we choose the assistive line to be $\partial\phi_0 : \alpha_b = 0$ (orange line in Figure 2(b)), such that along assistive line represents the gaits with straight fixed body.

The net displacement can be approximated by the path integral along the assistive line $\partial\phi_0$ plus the surface integral of the area enclosed by the gait path $\partial\phi$ and the assistive line (Gong et al., 2018):

$$\int_{\partial\phi} \boldsymbol{A}(\boldsymbol{r})d\boldsymbol{r} = \int_{\partial\phi_0} \boldsymbol{A}(\boldsymbol{r})d\boldsymbol{r} + \iint_{\phi-\phi_0} \nabla \times \boldsymbol{A}(\boldsymbol{r})d\alpha_b d\tau \tag{6}$$

where $\phi - \phi_0$ is the area enclosed by assitive line $\partial\phi_0$ and gait path $\partial\phi$. Note that when the gait path and the assistive line enclose disjointed areas in the shape space, the handedness (the direction of the curl) of these area enclosed can be

different. For example, as shown in our example in Figure 2(b), the assistive line (orange curve) and our gait path (blue curve) form two disjoint area: the area where $\partial\phi_0$ is above (blue shading area) and below (green shading area) $\partial\phi$. Thus, taking the handedness of enclosed area into consideration, the second term in (6) is computed as the surface integral of area where $\partial\phi$ is above $\partial\phi_0$ subtracted from the surface integral of area where $\partial\phi$ is below $\partial\phi_0$.

The physical meaning of the first term in (6) is the displacement resulting from leg movements while keeping the back fixed, i.e., the contribution solely from leg movements. It is independent from any gait path we design and can be pre-computed. The second term in (6) is the additional displacement resulting from coordinating body bending with leg movement. We can thus design the body bending according to our motion objectives.

We refer the reader to Gong et al. (2018) for a detailed derivation and proof of motion planning in a cylindrical shape spaces. In this way, the process for the gait design of legged systems is simplified to drawing a path in cylindrical shape space.

3.2. Periodic ground contacts

In legged systems, robots and animals repeatedly make and break contact with the environment. We introduce a binary *contact state variable*, $\boldsymbol{C}$, that describes the contact states: 0 (no contact, and therefore no contact forces) or 1 (full contact). Thus, the local connection becomes a function of both shape variables and contact states, i.e.,

$$\boldsymbol{\xi} = \boldsymbol{A}(\boldsymbol{r}, \boldsymbol{C})\dot{\boldsymbol{r}} \tag{7}$$

where shape variable $\boldsymbol{r} = [\alpha_b\ \beta_1\ \beta_2\ \beta_3\ \beta_4]^{\mathrm{T}}$ is a vector that includes the body bending joint angle (α_b, see Figure 1(c)) and the leg "shoulder" (shoulder for fore legs and hip for hind legs) joint angle ($\beta_i,\ i \in \{1, 2, 3, 4\}$, see Figure 1(c))

We assume that the contact variable $\boldsymbol{C}$ and the shape variable β_i can all be written as a function of leg phase τ, i.e.,

$$c_i = F_i(\tau), \quad \beta_i = f_i(\tau), \quad i = 1, 2, 3, 4 \tag{8}$$

As mentioned earlier, we prescribe the contact patterns, c_i, from existing knowledge of footfall sequence (see Figure 3). We use the contact state to prescribe the shoulder angle β_i. We enforce the β_i to be piecewise sinusoidal functions, partially because it permits the differentiability at transition. The specific shape of the sinusoid is chosen to respect the contact state of the foot, as depicted in Figure 3. The leg shoulder angle β_i is prescribed as piecewise sinusoidal function over either contact state or non-contact state with smooth connection. The generic examples of functions F_i and f_i are shown in Section 4 and Figure 3.

With leg movements prescribed by f_i and F_i, we can form a new shape space that consists of two variables α_b and τ, the body bending angle and the leg phase. This reduced shape space is parameterized by $\boldsymbol{\Omega} = [\alpha_b,\ \tau]^{\mathrm{T}}$. Note that according to the chain rule, we have

$$\dot{\boldsymbol{r}} = \frac{\boldsymbol{dr}}{\boldsymbol{d\Omega}}\frac{\boldsymbol{d\Omega}}{\boldsymbol{dt}} = \begin{bmatrix} 1 & 0 \\ 0 & \frac{df_1(\tau)}{d\tau} \\ 0 & \frac{df_2(\tau)}{d\tau} \\ 0 & \frac{df_3(\tau)}{d\tau} \\ 0 & \frac{df_4(\tau)}{d\tau} \end{bmatrix} \dot{\boldsymbol{\Omega}} \tag{9}$$

Therefore, we can rewrite (7) as

$$\boldsymbol{\xi} = \boldsymbol{A}(\boldsymbol{r}, \boldsymbol{C})\dot{\boldsymbol{r}} = A(\boldsymbol{\Omega})\frac{\boldsymbol{dr}}{\boldsymbol{d\Omega}}\dot{\boldsymbol{\Omega}} = \boldsymbol{A}'(\boldsymbol{\Omega})\dot{\boldsymbol{\Omega}} \tag{10}$$

where $\boldsymbol{A}'(\boldsymbol{\Omega})$ is the new local connection relating the reduced shape velocity $\dot{\boldsymbol{\Omega}}$ to body velocity $\boldsymbol{\xi}$. As one of the shape variables, τ, is periodic, the shape space is now cylindrical.

3.3. Granular RFT

Similar to prior work, we numerically derive $\boldsymbol{A}'$ using RFT (Li et al., 2013; Sharpe et al., 2015; Zhang and Goldman, 2014) to model the granular media that our system moves on. In this section, we provide a concise derivation of the local connection matrix needed for this article.

The GRF experienced by the locomotor is the sum of the GRF experienced by each body segment. RFT decomposes the resistive force experienced on an infinitesimally small portion of a locomotive intruder into two components: thrust (perpendicular) and drag (parallel), i.e.,

$$\boldsymbol{F} = \int (\boldsymbol{dF}_{\parallel} + \boldsymbol{dF}_{\perp}) \tag{11}$$

where $\boldsymbol{F}_{\parallel}$ and $\boldsymbol{F}_{\perp}$ denote forces parallel and perpendicular to a segment in contact with ground, respectively. During intrusions in granular media at slow speeds, the attack angle determines the $\boldsymbol{F}_{\parallel}$ and $\boldsymbol{F}_{\perp}$ on this body segment, i.e.,

$$\boldsymbol{F}_{\parallel} = \boldsymbol{F}_{\parallel}(\chi)$$
$$\boldsymbol{F}_{\perp} = \boldsymbol{F}_{\perp}(\chi)$$

where χ is the attack angle. Here $\boldsymbol{F}_{\parallel}$ and $\boldsymbol{F}_{\perp}$ are independent from the magnitude of the velocity (Zhang and Goldman, 2014).

Depending on the substrate, we can choose the corresponding RFT functions to approximate the GRFs. In our experiments, robots moved on poppy seeds, a model granular media (Li et al., 2013); therefore, we used the following previously suggested empirical functions to approximate $\boldsymbol{F}_{\perp}$ and $\boldsymbol{F}_{\parallel}$ (Mazouchova et al., 2013):

$$f_{\perp} = C\sin(\gamma)$$

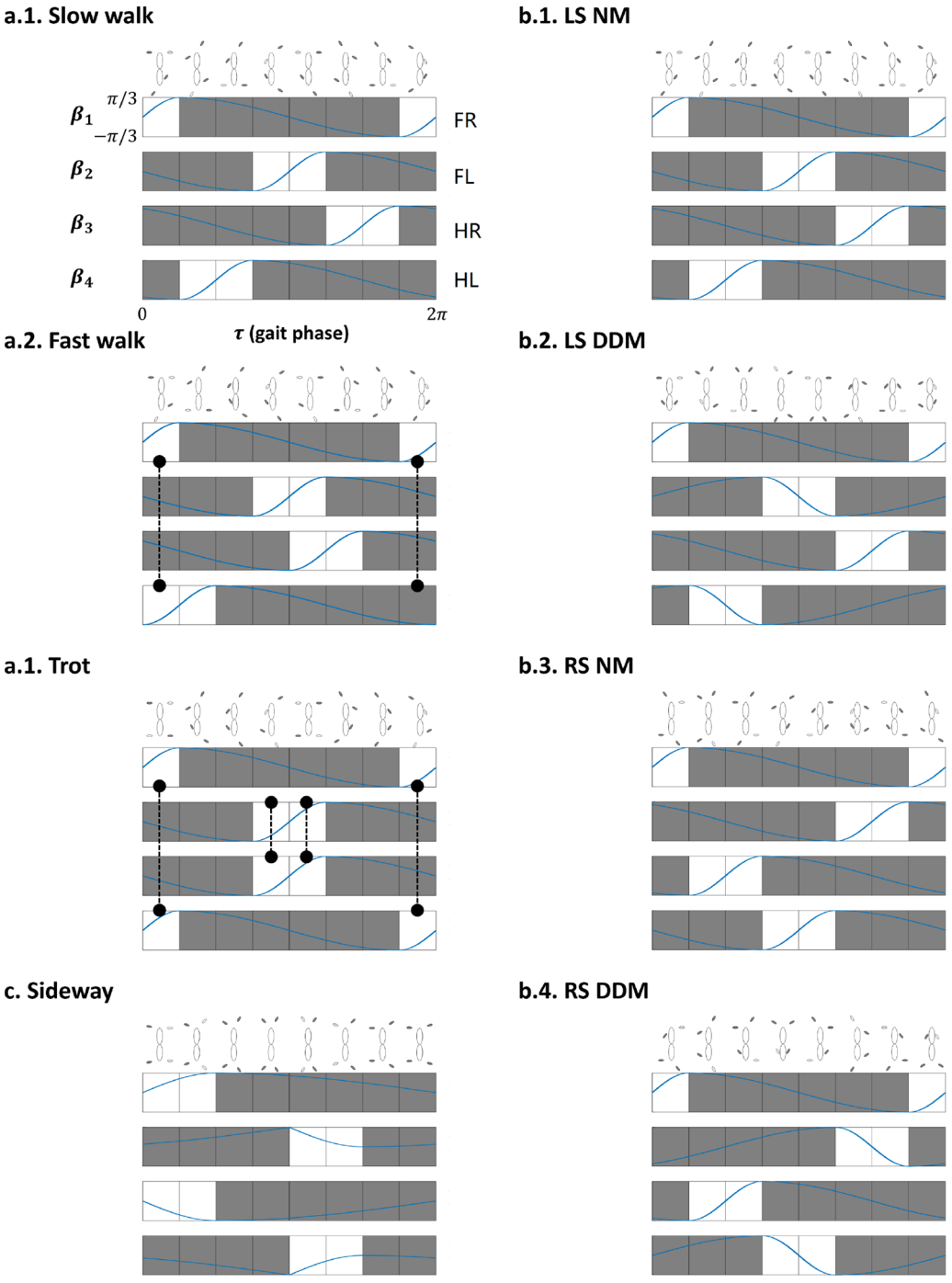

Fig. 3. The leg contact variables c_i and joint angles β_i prescribed by gait phase τ for (a.1) (forward) slow walk, (a.2) (forward) fast walk, (a.3) (forward) trot, (b.1) (rotational) lateral sequence with no modulation (**LS NM**), (b.2) (rotational) lateral sequence with differential drive modulation (**LS DDM**), (b.3) (rotational) rotary sequence with no modulation (**RS NM**), (b.4) (rotational) rotary sequence with differential drive modulation (**RS DDM**), and (c) (lateral) sideways leg movements. The "cartoon sequence" shows the leg joint angles and contact states (solid means contact; open in air) at different gait phases. A row of eight boxes indicates the contact state of a leg at eight different phases of the gait, where filled gray color represents contact and open white color represents non-contact state. The blue curves indicate the joint angles of the leg "shoulders" (shoulder for fore legs and hip for hind legs). The initials F, H, L, and R represent front, hind, left, and right leg, respectively. All the panels have the same ordinate range (from $-\frac{\pi}{3}$ to $\frac{\pi}{3}$) as in (a.1). The dashed lines in (a.2) and (a.3) indicate two legs are simultaneously in the air, which could only occur for diagonal leg pairs.

$$f_{\parallel} = A\cos(\gamma) + B(1 - \sin(\gamma)) + F_0$$

where $C = 0.66$, $A = 0.27$, $B = -0.32$, $F_0 = 0.09$ is the empirically (McInroe et al., 2016) fitted function to characterize the granular media resistant force.

Salamander animals moved on 300 μm glass particles, so we used the following previously suggested empirical functions to approximate $\boldsymbol{F}_{\perp}$ and $\boldsymbol{F}_{\parallel}$ (Schiebel et al., 2019):

$$f_{\perp} = a_0 + \sum_{i=1}^{2} a_i \cos(iw\gamma) + b_i \cos(iw\gamma)$$

$$f_{\parallel} = A_0 + \sum_{i=1}^{3} A_i \cos(iW\gamma) + B_i \sin(iW\gamma)$$

where $a_0 = 0.004041$, $a_1 = 0.0002925$, $b_1 = 0.002832$, $a_2 = -0.001038$, $a_2 = -0.0007345$, $w = 2$; $A_0 = -0.4833$, $A_1 = 0.3498$, $B_1 = 0.7504$, $A_2 = 0.2046$, $B_2 = -0.297$, $A_3 = -0.07208$, $B_3 = -0.009435$, and $W = 1.333$.

The attack angles χ of each segment can be calculated from the body velocity $\boldsymbol{\xi}$, body shape $\boldsymbol{\Omega}$, and shape velocity $\dot{\boldsymbol{\Omega}}$ (Murray et al., 1994). By assuming that the motions of quadrupeds in granular material are quasi-static (Gong et al., 2016), we consider the total net force applied to the system is zero:

$$\boldsymbol{F} = \int (d\boldsymbol{F}_{\parallel}(\boldsymbol{\xi}, \boldsymbol{\Omega}, \dot{\boldsymbol{\Omega}}) + d\boldsymbol{F}_{\perp}(\boldsymbol{\xi}, \boldsymbol{\Omega}, \dot{\boldsymbol{\Omega}})) = \boldsymbol{0} \qquad (12)$$

At a given body shape $\boldsymbol{\Omega}$, Equation (12) connects the shape velocity $\dot{\boldsymbol{\Omega}}$ to the body velocity $\boldsymbol{\xi}$. Therefore, by linearizing (12), we can numerically derive the local connection matrix $\boldsymbol{A}'(\boldsymbol{\Omega})$. In our implementation, we compute the root of (12) using the MATLAB function *fsolve*.

With these assumptions, the local connection of a quadrupedal robot moving in granular media can be approximated by numerically calculating displacements in the body frame. We refer the reader to Gong et al. (2016) for detailed numerical calculations. This numerically determined local connection can be used to plot connection vector fields and height functions.

3.4. Gait design

Note that 2D cylindrical shape space is a simple representation that includes both body bending and leg movements. Compared with higher-dimensional systems, the 2D shape space has the advantage of allowing visual gait analysis, as we can design gaits by looking at the height functions. To achieve such simple representation, we made many assumptions (e.g., using one-DoF body joint to represent the body bending in sprawled posture quadrupedal locomotion) to perform dimensionality reduction.

With the height function, one can design gaits by drawing a path through the shape space. The periodic gait path is assumed to be described by Fourier series. To limit the number of parameters to be optimized while maintaining the flexibility of the gait design (Alexander, 1984), we keep the first two orders of the Fourier series in our prescription, i.e.,

$$\partial\phi_{a_i,b_i} = \{[\alpha_b,\ \tau] : \alpha_b = \sum_{n=1}^{n=2} a_n \cos(n\tau + b_n)\} \qquad (13)$$

We denote $\partial\phi_{a_i,b_i}$ as $\partial\phi_{a_1,a_2,b_1,b_2}$ to simplify notation. Finally, we maximize the area enclosed by gait path and the assistive line by optimizing over the parameters a_i and b_i:

$$\text{argmax} \iint_{\phi_{a_i,b_i} - \phi_0} \boldsymbol{H} d\alpha_b d\tau$$

$$\text{subject to } \max_{\phi_{a_i,b_i}} \alpha_b < \Gamma_\alpha$$

where $\boldsymbol{H} = \boldsymbol{H_x}$, $\boldsymbol{H_y}$ *or* $\boldsymbol{H_\theta}$ depending on the direction of gait that we wish to design motion; Γ_α is the body bending joint angle limit.

Figure 4 shows several examples of gaits on height functions for a variety of maneuvers. In summary, our approach uses the steps given in Figure 5.

4. Analytical results

4.1. Forward height functions

We studied how body bending, coordinated with leg movements, improved the forward displacement per gait cycle. We first prescribed three typical types of leg movements, taken from prior work (Hildebrand, 1965), that will result in forward displacement.

The three types of leg movements prescribed in this section are slow walk, fast walk, and trot. Inspired by Hildebrand's analyses (Hildebrand, 1965), we classified these gaits with two parameters: lateral leg phase shift (the fraction of the step cycle that hind limbs lead the fore limbs on the same side) and duty factor (the fraction of the step cycle where the foot is on the ground). The duty factors for the three gaits are all 0.75, and the lateral leg phase shifts are 0.25, 0.375, and 0.5, respectively. Each of these parameter choices leads to a specific footfall pattern which can be seen in Figure 3(a). The leg "shoulder" joint angles are prescribed as piecewise sinusoidal functions which move from cranial end to caudal end when the leg makes contact with ground, and move from caudal end to cranial end when the leg is in the air (Figure 3(a)). We set the body bending joint angle limit $\Gamma_\alpha = \frac{\pi}{3}$ in this section unless otherwise noted.

The **slow walk** (lateral leg phase shift = 0.25) is a four-beat[2] gait with evenly spaced leg lifting following the sequence fore right, hind left, fore left, hind right (defined as lateral sequence (**LS**) (Hildebrand, 1965). The **fast walk** (lateral leg phase shift = 0.375) is another four-beat gait following the lateral sequence. Unlike the slow walk gait, there is an overlap of the aerial phase between fore right

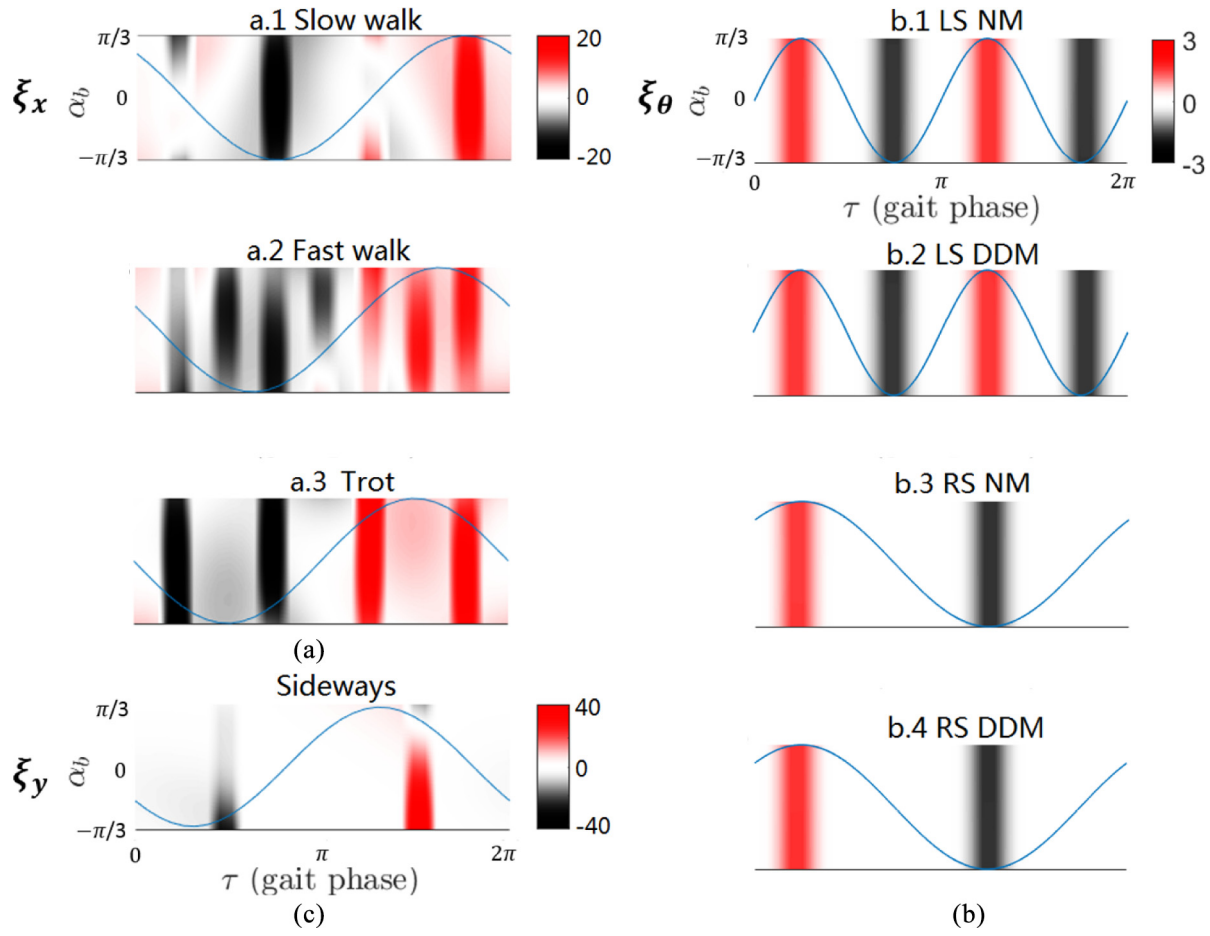

Fig. 4. Height functions. (a) Forward height functions associated with trot (a.1), fast walk (a.2), and slow walk (a.3) leg movements. The unit of colorbar is centimeters per step, i.e., cm $/4\pi^2$. (b) Rotational height functions associated with lateral sequence no modulation (**LS NM**) (b.1), lateral sequence differential drive modulation (**LS DDM**) (b.2), rotary sequence no modulation (**RS NM**) (b.3), and rotary sequence differential drive modulation (**RS DDM**) (b.4) leg movements. The unit of colorbar is radians per step, i.e., rad $/4\pi^2$. (c) Lateral height function associated with sideways leg movements. The blue curves are the identified "optimal" gait paths. Red, white, and black indicate positive, zero and negative values, respectively. The ordinate range is same for all panels. The unit of colorbar is centimeters per step, i.e., cm $/4\pi^2$.

and hind left legs (as well as fore left and hind right). The **trot gait** (lateral leg phase shift = 0.5) is a two-beat gait with diagonally paired leg movement. The fore right leg is always in phase with the hind left leg; while the fore left leg is always in phase with the hind right leg. The detailed descriptions of these gaits are presented in Figure 3(a). Note that the overlaps in diagonal-leg (the FR–HL pair or FL–HR pair) non-contact state increase from slow walk, fast walk to trot, which leads to higher speeds.

We can coordinate body bending to improve forward displacements per gait cycle by investigating the forward height functions. The forward height functions for these leg movements are shown in (Figure 4(a)). The gait paths with the maximum surface integral in the forward height functions ("optimal" gaits) are predicted to be the gaits with the largest forward displacement per gait cycle. We also identified the worst body bending coordination with the minimal surface integrals ("worst" gaits). We tested the "neutral" gaits with fixed straight back ($\alpha_b = 0$) for reference.

We observed that body bending that optimizes the forward displacement per gait cycle is dominated by the first term of the Fourier series, in which case a_1 tends to Γ_a and a_2 tends to 0. However, the optimized b_1 s vary for fast walk, slow walk, and trot leg movements.

4.2. Rotational height functions

Next, we studied the role of body bending in rotational motions. Four types of leg movements were prescribed: the lateral footfall sequence with no modulation (Figure 3(b.1)), the lateral footfall sequence with differential drive modulation (Figure 3(b.2)), the rotary footfall sequence with no modulation (Figure 3(b.3)), and the rotary footfall sequence with differential drive modulation (Figure 3(b.4)).

4.2.1. Lateral sequence and rotary sequence. Although the lateral sequence (FR–HL–FL–HR) (**LS**) footfall pattern is widely used in forward walking, we show that by properly

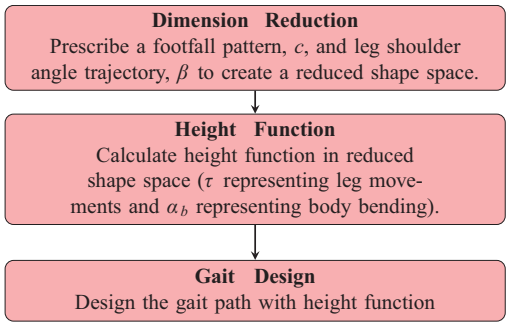

Fig. 5. The flow chart of our gait design process.

coordinating body bending, the **LS** footfall pattern can also give rise to rotational motion (e.g., turning). As expected, other sequences favor motions in other directions. Hirose et al. (1986) introduced *rotary sequence footfall pattern* (FR–HR–HL–FL) (**RS**) that favors counterclockwise turning. In this section, we prescribed both **LS** and **RS** to produce rotational motions. The leg movements prescribed in Figure 3(b.3) and (b.4) followed the (**RS**) footfall pattern.

4.2.2. Differential drive modulation and no modulation. In this section, we introduce the notion of modulation of the joint amplitudes to cause rotational motion as well. To distinguish modulated motion with no modulated motion, we use the abbreviation **NM** to mean no modulation. In no modulation (**NM**) leg movements, the leg "shoulder" joint angles are prescribed as piecewise sinusoidal functions as mentioned in Section 4.2.1 (move from cranial end to caudal end when the leg makes contact with ground, and move from caudal end to cranial end when the leg is in the air) (see Figure 3(b.1) and (b.3)). Leg movements previously prescribed in **NM** will lead to pure forward translation and no rotation. However, rotation can be introduced by coordinating body undulation.

Now we define differential drive modulation (**DDM**) leg movements. The leg "shoulder" angles are also prescribed as piecewise sinusoidal functions. However, the right (FR and HR) limb joint angles move from cranial end to caudal end when the leg makes contact with ground, and move from caudal end to cranial end when the leg is in the air; while the left (FL and HL) limb joint angles move from caudal end to cranial end when the leg makes contact with ground, and move from cranial end to caudal end when the leg is in the air (see Figure 3(b.2) and (b.4)). In this way, the differential on lateral limb amplitude is modulated to introduce rotational motion (Dudek and Jenkin, 2010). We term counterclockwise (**CCW**) rotation as the positive direction. The differential drive modulated leg movements can lead to pure **CCW** rotation without translation. Properly coordinating body undulation will further increase the rotation per gait cycle.

Note that in Section 4.1, we prescribe the leg movement without modulating the leg amplitude. Therefore, they are in the category of no modulation. In addition, prescribed leg movements of the slow walk gait in Section 4.1 (Figure 3(a.1)) are identical to the prescribed **LS** leg movements with **NM** (**LS NM**) in this subsection (Figure 3(b.1)). We show that body undulation can lead to either additional rotation or additional forward displacement to the original leg movements (see Figure 6).

4.2.3. Body undulation during rotation. In addition to modulating the amplitudes, we can also design the turning motions by investigating the rotational height functions. The rotational height functions are presented in Figure 4(b). The gait paths that enclose the maximum surface integral in the rotational height functions are predicted to be the gaits with the maximum **CCW** rotation per gait cycle ("optimal" gait). Similarly, the gait paths that enclose the minimum surface integral in the rotational height functions are predicted to be the gaits with the minimum **CCW** (i.e., the maximum **CW**) rotation ("worst" gait). Interestingly, the body bending in coordination with **LS** that optimizes rotation is dominated by the second term of Fourier series, whereas the body bending in coordination with **RS** that optimizes rotation is dominated by the first term of Fourier series.

4.2.4. Steering. In Section 4.2.2, we showed that with the help of body bending, quadrupedal systems can simultaneously go forward and rotate; we call this type of motion steering because it is reminiscent of a car driving down the street. In this section, we show that properly coordinated body bending can control the steering angle of quadrupedal systems. The leg movements in this section are prescribed by slow walk (**NM LS**).

One of the most important parameters in steering is the turning radius. As illustrated in (Figure 7), the quadrupeds that walks and turns simultaneously will essentially follow a circle. The turning radius, R, is given by

$$R = \frac{D \cdot \sin\left(\frac{\pi-\theta}{2}\right)}{\sin(\theta)}, \tag{14}$$

where D is the stride displacement (displacement per gait cycle) and θ is the stride rotation (body rotation per gait cycle).

Next, we aim to control the turning radius by modulating the body bending. From the rotational height function in Figure 4(b.1), we observe that the surface integral enclosed by the assistive line and the gait path will increase with body joint angle amplitude. However, that path in Figure 4(b.1) will enclose no additional area in its corresponding forward height function Figure 4(a.1). Thus by increasing the body bending joint angle amplitude, Γ_α, greater stride rotation, θ, is expected while stride displacement D remains constant. In this way, we show that we can control the turning radius by modulating the body bending amplitude.

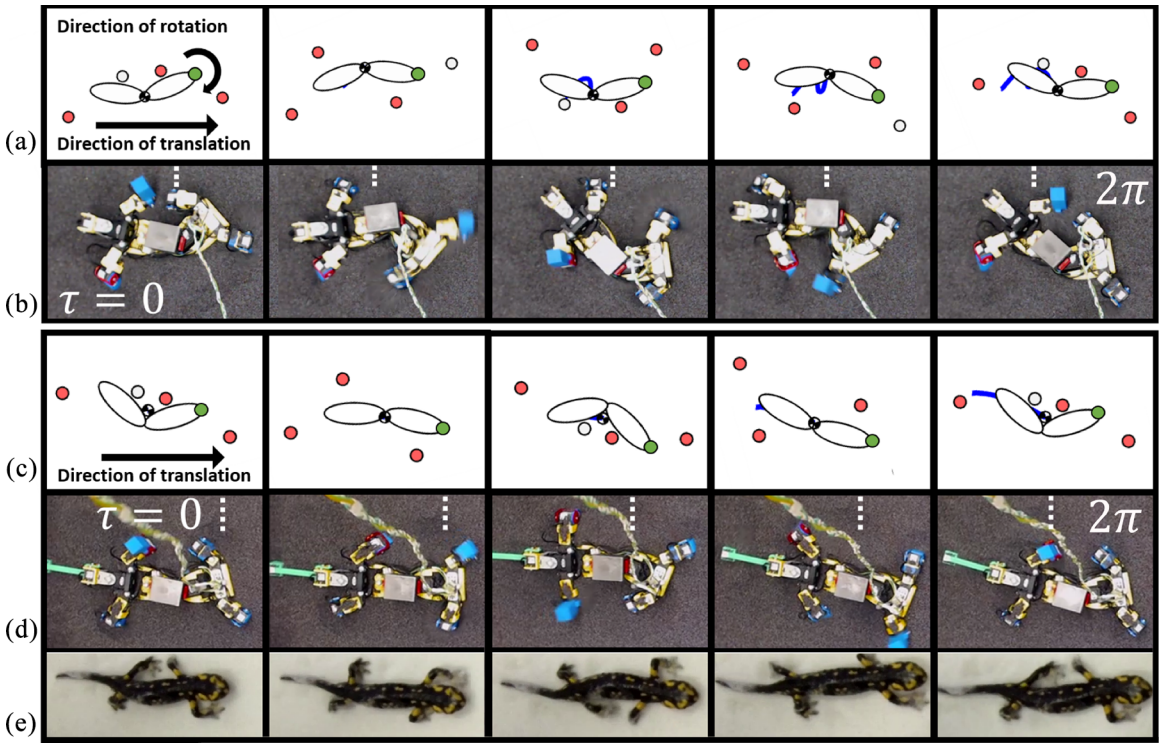

Fig. 6. Snapshots of robot experiment (b), (d), RFT simulation (a), (c), and animal experiments (e). Body bending coordinated with leg movements (a), (b) changes the orientation of the body or increases forward displacement. In (a) and (c), the green dots identify the head and the solid blue line represents the trajectory of center of mass. In (b) and (d), the module connected to hanging tail (not making contact with the ground) indicates the hind body module. We compared our designed forward gaits (c), (d) with the forward locomotion observed in animal experiments (e).

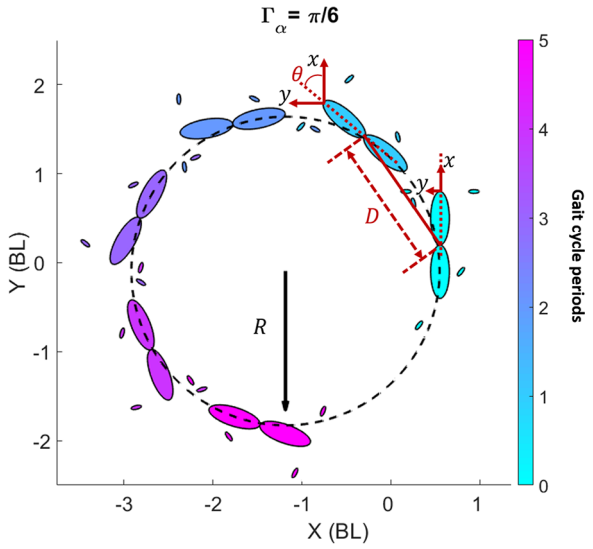

Fig. 7. Snapshots of robot simulation following a circle. Rotation with forward motion will lead to an arc in center of mass trajectory. Here R is the curvature radius of the center of mass trajectory; θ is the stride rotation and D is the stride displacement.

4.3. Lateral height function

Finally, we studied how properly coordinated body bending can improve lateral displacement per gait cycle. Hirose et al. (1986) introduced the footfall patterns that produce slight lateral motion, in which the fore right leg is in phase with the hind right leg, and the fore left leg is in phase with the hind left leg. The detailed description of leg movements is shown in Figure 3(c). We then calculate lateral height functions (Figure 4(c)).

The gait path with maximum surface integral in the height function ("optimal" gait) is predicted to be the gait with the largest lateral displacement per gait cycle. We also identified the body bending that corresponds to the minimal surface integral ("worst" gait). We tested the "neutral" gait with fixed straight back ($\alpha_b = 0$).

Quadrupeds have limited ability to move sideways (Carbone and Ceccarelli, 2005). However, body bending will greatly enhance the ability of a quadrupedal robot to move laterally. In the next section, we show the lateral displacement for optimal, neutral, and worst body bending in coordination with leg movements across granular media.

5. Experimental results

To verify and explore our theoretical model predictions, we developed a robophysical model (Aguilar et al., 2016; Ozkan-Aydin et al., 2017; Ozkan-Aydin et al., 2019). Specifically, we built a quadrupedal robot (Figure 1(a)) and tested its performance on granular media. This open-loop,

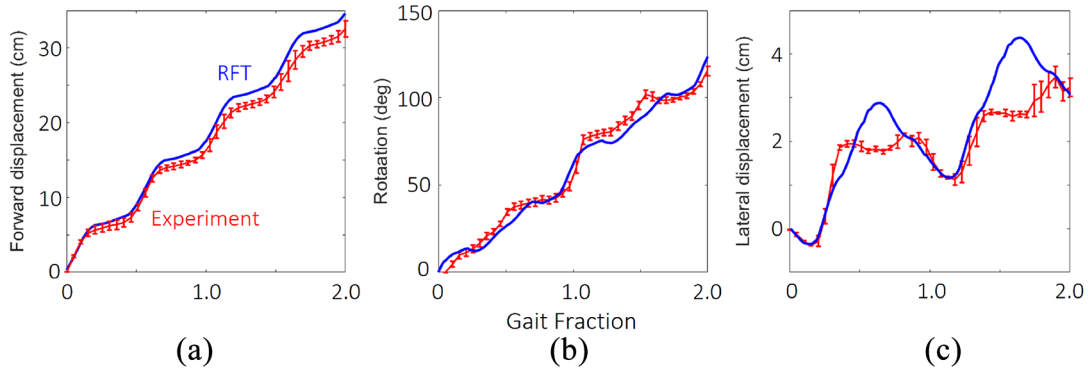

Fig. 8. Sample trajectories of robot experiments and RFT simulations implementing (a) fast walk gait, (b) rotary sequence no modulation gait, and (c) sideways gait, showing close agreement between RFT simulations and robot experiments. In these gaits, body undulations are properly designed to improve (a) forward, (b) rotational, and (c) lateral displacements.

servo-driven, 3D-printed robot (450 g, ~40 cm long) has four legs and an actuated back. Each leg has two servo motors (XL-320) to control its vertical position and its lateral position. A joint in the middle of the body (AX-12 servo) controls lateral body bending.

Using a fully automated setup (Ozkan-Aydin et al., 2017; Qian et al., 2013), we experimentally and systematically tested the role of body bending during quadrupedal locomotion on a bed filled with ~1 mm diameter poppy seeds. We performed three trials for each gait, with each trial consisting of at least three complete gait periods. The robot executed a programmed set of movements to move on the loosely packed poppy seeds. Throughout the experiment, four Optitrack Flex13 cameras recorded the positions of infrared-reflective markers on the robot (at 120 frames per second (FPS)). At the end of each experiment, the robot's final position was identified. A three-axis motor system moved to the robot, picked it up, and sent it back to the starting position. Before each experiment, an air-fluidized bed erased the footprints and allowed the seeds to be reset into a loosely packed state (Li et al., 2009).

We provide snapshots of the robot executing gaits predicted by geometric mechanics in Figure 6. We compared the trajectories of quadrupedal robot experiments and RFT simulations in Figure 8, and show that they are in good agreement (Figure 9). Note that in Figure 8c, there is deviation between the robot experiments and RFT simulation. We believe that the relatively shorter displacement in a robot experiment is due to the poppy seed accumulation that is not modeled in RFT simulation.

5.1. Robot experiment verification of forward height function prediction

In Section 4.1, we identified the "optimal," "neutral," and "worst" body bending from forward height functions to improve forward displacement per gait cycle. We verified the predictions from forward height functions by RFT simulations and robot experiments across granular materials. Both RFT simulations and robot experiments suggest that the "optimal" body–leg coordination can improve the forward displacement, whereas the "worst" phasing can lead to ineffective forward gait. Simulation and experiment data are presented in Figure 9(a).

5.2. Robot experiment verification of rotational motions

5.2.1. Lateral sequence and rotary sequence. In Section 4.2, we identified the "optimal," "neutral," and "worst" body bending from rotational height functions in coordination with **LS** and **RS**. We verified predictions from rotational height functions by RFT simulations and robot experiments across granular materials. The data are presented in Figure 9(b). Both RFT simulations and robot experiments suggested that proper body–leg coordination can improve the **CCW** rotation.

5.2.2. Differential drive modulation and no modulation. From Figure 9(b), we observed that when the body is maintained fixed straight (i.e., the "neutral" body bending), the **DDM** leg movements lead to pure rotation without translation whereas **NM** leg movements lead to pure translation without rotation.

In leg movements prescribed in **DDM**, the "optimal" body bending coordination can improve the body orientation rotation per gait cycle (good in place turn) whereas "worst" body bending can decrease the body orientation rotation per gait cycle (bad in place turn).

In leg movements prescribed in **NM**, the "optimal" body bending coordination will introduce counterclockwise rotation to forward motion (counterclockwise steering) whereas "worst" body bending will introduce clockwise rotation to forward motion (clockwise steering).

5.2.3. Steering. We further verified our steering radius control hypothesis with robot experiments and RFT simulation. We plotted the body bending amplitude Γ_α against

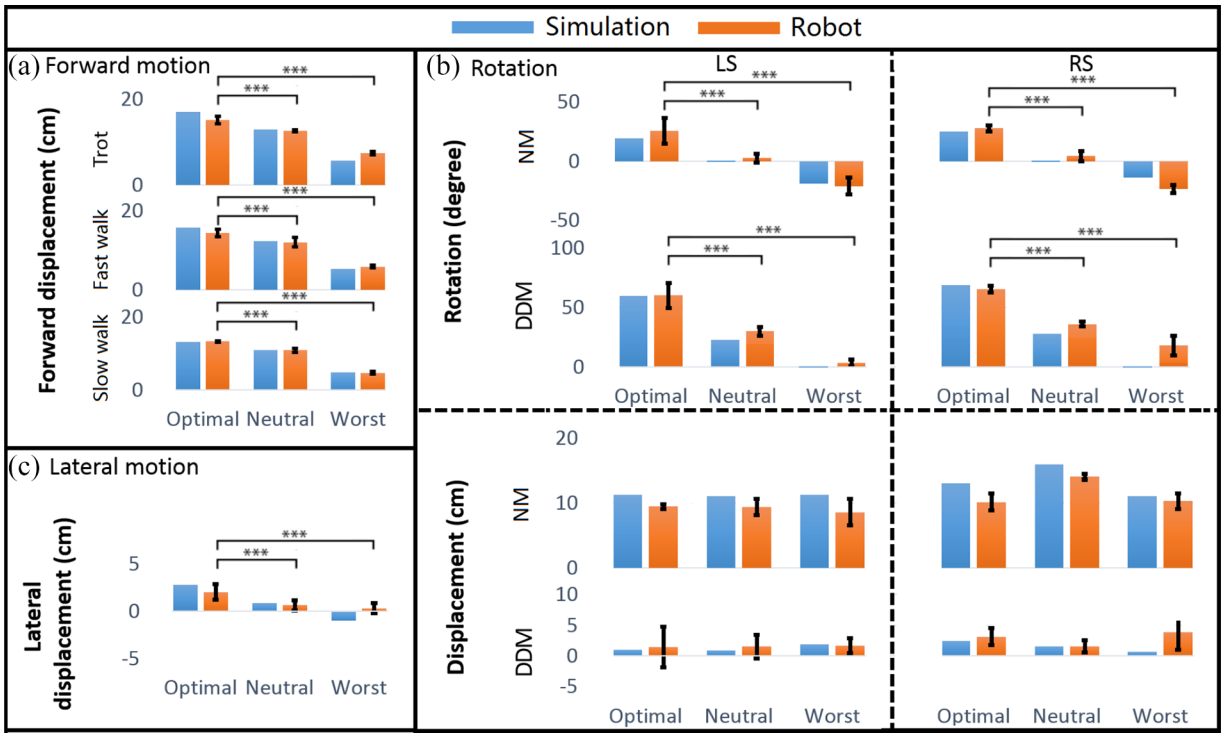

Fig. 9. Comparison of displacement in RFT simulations (blue bars) and robot experiments (orange bars with error bar, representing 1 standard deviation) results of (a) forward, (b) rotational, and (c) lateral gaits, showing close agreement between RFT simulations and robot experiments. Each gait is tested for ~3 experiment trials; each trials containing at least ~3 gait periods. The "optimal," "neutral," and "worst," respectively, represent the optimal body bending, no body bending (fixed straight back), and the worst body bending. We indicate statistically significant improvement (Sprinthall and Fisk, 1990) comparing the "optimal"–"neutral," as well as "optimal"–"worst" gaits. The gait comparison with a horizontal bracket with *** represents statistically significant improvement ($p<0.001$); the gait comparison without a horizontal bracket represents no statistically significant improvement ($p>0.05$). For rotational gaits in (b), we show both transitional and rotational displacement values for completeness only: body bending is optimized with respect to rotation only, and displacement changes are not optimized.

the turning radii in Figure 10. Both robot experiments and simulations suggested that by modulating the body bending joint angle amplitude, we can control the turning radius. Note that the simulation–experiments discrepancy increases at larger amplitude. As our robot experiments were performed on granular media, there can be granular material accumulation on the side when robots exhibits large turns. The accumulated granular material can have greater effect on the locomotion performance when the robots implement multiple gait cycles. Therefore, we suspect that the granular material accumulation that lead to underperformance of steering experiments in Figure 10.

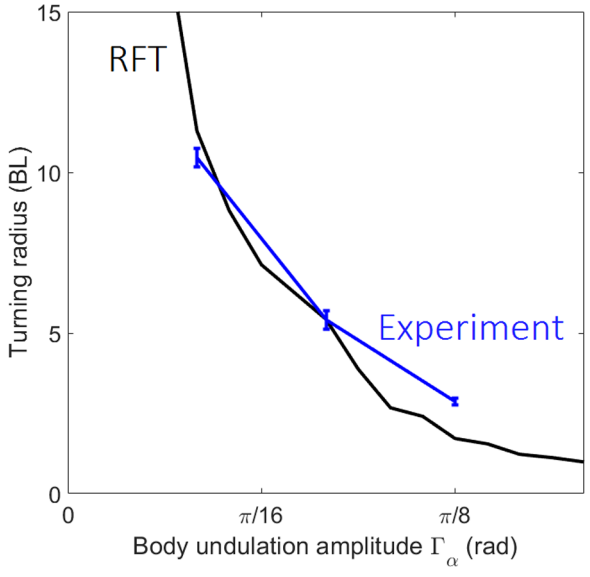

Fig. 10. Body undulation amplitude versus robot turning radii (the curvature radius of the center of mass motion trajectory). We hypothesize that by modulating the body undulation amplitude, we can control the turning radius of the robot. Robot experimental data (blue) and RFT simulation data (black) validate our hypothesis.

5.3. Robot experiment verification of lateral height function prediction

Finally, we identified the "optimal," "neutral," and "worst" body bending from lateral height functions to improve lateral displacement per gait cycle. We verified predictions from lateral height functions using RFT simulations and robot experiments across granular materials. Both RFT simulations and robot experiments suggest that the "optimal" body–leg coordination can improve the lateral

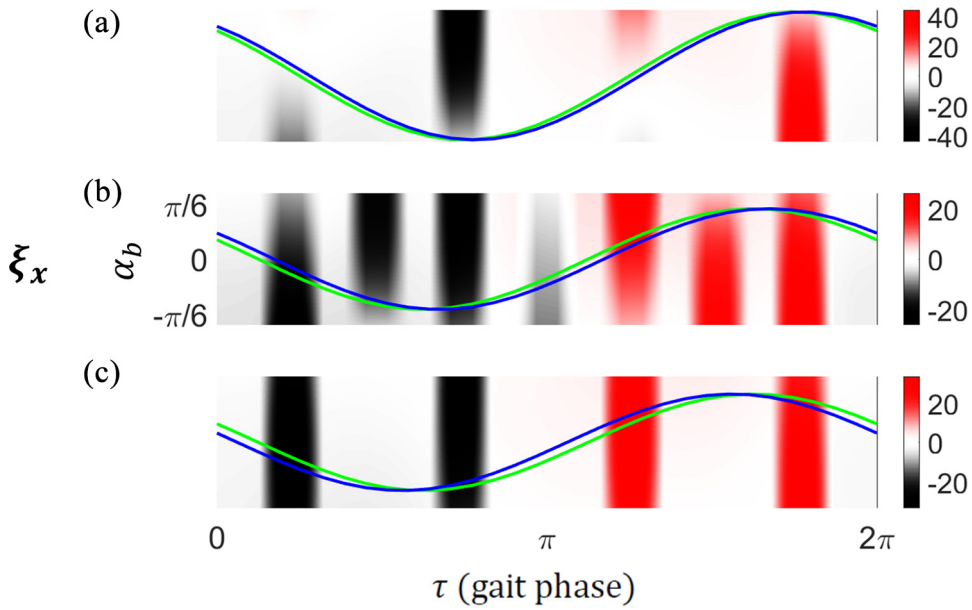

Fig. 11. Height functions for salamanders, namely experimentally measured gaits for (a) slow walk, (b) fast walk, and (c) trot, with salamander gait in blue curves and geometric mechanics predicted gait in green curves overlaid. All the panels have the same body angle range as in the middle panel.

displacement, whereas the "worst" phasing can lead to an ineffective lateral gait. Simulation and experiment data are presented in Figure 9(c).

5.4. Animal experiment verification of forward height function prediction

To extend our study to biological quadrupedal systems, we collected data and performed analysis on fire salamanders (*S. salamandra*) to investigate whether the animal uses body kinematics to optimize the forward motion.

In these experiments, individual animals walked along a straight trackway filled with 300 μm glass particles. Three cameras (GoPro Hero3+, 720 pixel resolution) were positioned around the trackway and recorded synchronized videos at 120 FPS. All experiments were approved by the Royal Veterinary College's Clinical Research Ethical Review Board, approval number 2015 1336. No animals were harmed for the experiments, and animals had rest periods in between data collection trials. Experiments were conducted in a humidity-controlled laboratory at the University of Oviedo, Spain. The temperature (~18°C) and light cycle (12 h:12 h dark:light) were maintained at constant levels.

At least three gait periods were recorded in each experiment. Limb positions, body angles, and footfall timing are manually extracted from each recording. According to the limb positions and footfall timing, we selected three representative salamander motion videos (each contains at least three gait periods of animal motion), which correspond to "trot" (duty factor 0.75±0.03, lateral leg phase shift 0.25±0.05), "fast walk" (duty factor 0.76±0.04, lateral leg phase shift 0.36±0.02), and "slow walk" gaits (duty factor 0.73±0.1, lateral leg phase shift 0.50±0.02). We fitted the animal body angles with the first two terms of Fourier series as in (13). We plotted the obtained animal body bending angles as a function of the leg movement phase (blue curves in Figure 11).

To predict the proper body bending coordination with "trot," "slow walk," and "fast walk" salamander leg movements, we calculated the corresponding forward height functions. In the forward height function, we then can design and predict the body bending gait paths to maximize forward displacements. The green curves in Figure 11 are the predicted body bending gait paths with body-bending amplitudes Γ_α extracted experimental data. We show that the body–leg coordination gait paths in salamander locomotion are in close agreement with our theoretical prediction to maximize forward displacement.

6. Conclusion

In this article, we have studied the role of body bending during quadrupedal locomotion. We took a modeling approach that had been previously limited to low-DoF walking systems and idealized contact with environment and extended this modeling approach to a quadrupedal system with a single internal DoF in its back moving on deformable terrains. Our approach can also be applied to other systems where the frictional forces dominate the inertial forces, such as Coulomb friction dominated systems (Rieser et al., 2019).

Our theory has been verified by RFT simulation and robot experiments. Furthermore, we have also observed that our calculated body bending coordination to improve

forward displacements are close to those from animal locomotion experiments. In addition to these examples, by varying the body bending amplitude, we have been able to regulate the turning radii, which can provide primitives for path planning and motion planning and control.

In contrast to the feedback control algorithms in a CPG system, our gait design algorithms do not require prior knowledge of gait formula. However, we believe that our approach could be used as a basis for CPG-based approaches. That is, our gait design process can be used to generate and optimize gait trajectories, which can then be tracked online by a set of coupled oscillators.

In addition, our methods focused primarily on the kinematics aspect of locomotion. Although we assumed the robots have quasi-static motion, our methods can be applied to robots moving as fast as ~0.3 body lengths per second. Although our methods cannot directly be applied to the dynamic locomotion systems, our observations of kinematics of locomotion can provide guides to dynamic motions.

Finally, our methods of coordinating body bending can extend to other morphologies. Future work could consider other types of bends, which may be represented by modal functions, along with other morphologies that may benefit from body bending. Future work could also include a systematic study of animal whole-body coordination and evaluate it in terms of speed, stability, and cost of transport.

Acknowledgements

We would like to thank Feifei Qian for early design of the experimental setup, Ariel Koh for construction of the new gantry system, and Enes Aydin for preparing the supplementary movie.

Funding

The author(s) disclosed receipt of the following financial support for the research, authorship, and/or publication of this article: This article was supported by the NSF (grant number PoLS PHY-1205878) and ARO (grant number W911NF-11-1-0514).

Notes

1. In actuality, the connection vector field is a one-form (a co-vector field) and instead of looking for dot products, we are looking for the naturally pairing between co-vectors and vectors that produce scalars. Here, our use of the term dot-product is more of a visualization "convenience."
2. Imagine each leg placement is like beating a drum. For the slow walk gait, one would hear four separate beats of the drum as the leg makes contact with the ground. A trot gait is a two-beat gait.

ORCID iDs

Baxi Chong https://orcid.org/0000-0002-6187-4911
Jeffery W. Rankin https://orcid.org/0000-0002-6639-8280

References

Aguilar J, Zhang T, Qian F, et al. (2016) A review on locomotion robophysics: the study of movement at the intersection of robotics, soft matter and dynamical systems. *Reports on Progress in Physics* 79(11): 110001.

Alexander RM (1984) The gaits of bipedal and quadrupedal animals. *The International Journal of Robotics Research* 3(2): 49–59.

Altendorfer R, Moore N, Komsuoglu H, et al. (2001) RHex: A biologically inspired hexapod runner. *Autonomous Robots* 11(3): 207–213.

Astley HC, Mendelson JR, Dai J, et al. (2020) Surprising simplicities and syntheses in limbless self-propulsion in sand. *Journal of Experimental Biology* 223(5): jeb103564.

Bai S, Low KH, Seet G and Zielinska T (1999) A new free gait generation for quadrupeds based on primary/secondary gait. In: *Proceedings 1999 IEEE International Conference on Robotics and Automation*, Vol. 2, pp. 1371–1376.

Batterman RW (2003) Falling cats, parallel parking, and polarized light. *Studies in History and Philosophy of Science Part B: Studies in History and Philosophy of Modern Physics* 34(4): 527–557.

Bien Z, Chun MG and Son HS (1991) An optimal turning gait for a quadruped walking robot. In: *Proceedings IEEE/RSJ International Workshop on Intelligent Robots and Systems '91 "Intelligence for Mechanical Systems" (IROS '91)*, Vol. 3, pp. 1511–1514.

Bloch AM, Krishnaprasad PS, Marsden JE and Murray RM (1996) Nonholonomic mechanical systems with symmetry. *Archive for Rational Mechanics and Analysis* 136(1): 21–99.

Buchli J, Kalakrishnan M, Mistry M, Pastor P and Schaal S (2009) Compliant quadruped locomotion over rough terrain. In: *2009 IEEE/RSJ International Conference on Intelligent Robots and Systems*, pp. 814–820.

Buehler M, Battaglia R, Cocosco A, Hawker G, Sarkis J and Yamazaki K (1998) SCOUT: A simple quadruped that walks, climbs, and runs. In: *Proceedings 1998 IEEE International Conference on Robotics and Automation*, Vol. 2, pp. 1707–1712. IEEE.

Buehler M, Cocosco A, Yamazaki K and Battaglia R (1999) Stable open loop walking in quadruped robots with stick legs. In: *Proceedings 1999 IEEE International Conference on Robotics and Automation*, Vol. 3, pp. 2348–2353. IEEE.

Carbone G and Ceccarelli M (2005) Legged robotic systems. In: *Cutting Edge Robotics*. InTech.

Cham JG, Karpick JK and Cutkosky MR (2004) Stride period adaptation of a biomimetic running hexapod. *The International Journal of Robotics Research* 23(2): 141–153.

Cho DJ, Kim JH and Gweon DG (1995) Optimal turning gait of a quadruped walking robot. *Robotica* 13(6): 559–564.

Crespi A, Karakasiliotis K, Guignard A and Ijspeert AJ (2013) Salamandra Robotica II: An amphibious robot to study salamander-like swimming and walking gaits. *IEEE Transactions on Robotics* 29(2): 308–320.

Cruse H (1990) What mechanisms coordinate leg movement in walking arthropods? *Trends in Neurosciences* 13(1): 15–21.

Daan S and Belterman T (1968) Lateral bending in locomotion of some lower tetrapods. I.2. *Proceedings of the Koninklijke Nederlandse Akademie van Wetenschappen series C - Biological and Medical Sciences* 71(3): 245.

Dai J, Faraji H, Gong C, Hatton RL, Goldman DI and Choset H (2016) Geometric swimming on a granular surface. In: *Robotics: Science and Systems*.

Dudek G and Jenkin M (2010) *Computational Principles of Mobile Robotics*. Cambridge: Cambridge University Press.

Eckert P, Spröwitz A, Witte H and Ijspeert AJ (2015) Comparing the effect of different spine and leg designs for a small bounding quadruped robot. In: *2015 IEEE International Conference on Robotics and Automation (ICRA)*, pp. 3128–3133. IEEE.

Farley CT and Ko TC (1997) Mechanics of locomotion in lizards. *Journal of Experimental Biology* 200(16): 2177–2188.

Frolich LM and Biewener AA (1992) Kinematic and electromyographic analysis of the functional role of the body axis during terrestrial and aquatic locomotion in the salamander *Ambystoma tigrinum. Journal of Experimental Biology* 162(1): 107–130.

Full RJ and Koditschek DE (1999) Templates and anchors: neuromechanical hypotheses of legged locomotion on land. *Journal of Experimental Biology* 202(23): 3325–3332.

Gong C, Goldman DI and Choset H (2016) Simplifying gait design via shape basis optimization. In: *Robotics: Science and Systems*.

Gong C, Whitman J, Grover J, Chong B, Ren R and Choset H (2018) Geometric motion planning for systems with toroidal and cylindrical shape spaces (submitted). In: *Dynamic Systems and Control Conference*.

Hatton RL and Choset H (2015) Nonconservativity and noncommutativity in locomotion. *The European Physical Journal Special Topics* 224(17): 3141–3174.

Hatton RL, Ding Y, Choset H and Goldman DI (2013) Geometric visualization of self-propulsion in a complex medium. *Physical Review Letters* 110(7): 078101.

Hildebrand M (1965) Symmetrical gaits of horses. *Science* 150(3697): 701–708.

Hirose S, Kikuchi H and Umetani Y (1986) The standard circular gait of a quadruped walking vehicle. *Advanced Robotics* 1(2): 143–164.

Holmes P, Full RJ, Koditschek D and Guckenheimer J (2006) The dynamics of legged locomotion: Models, analyses, and challenges. *SIAM Review* 48(2): 207–304.

Horvat T, Melo K and Ijspeert AJ (2017) Spine controller for a sprawling posture robot. *IEEE Robotics and Automation Letters* 2(2): 1195–1202.

Ijspeert AJ (2020) Amphibious and sprawling locomotion: From biology to robotics and back. *Annual Review of Control, Robotics, and Autonomous Systems* 3: 173–193.

Ijspeert AJ, Crespi A, Ryczko D and Cabelguen JM (2007) From swimming to walking with a salamander robot driven by a spinal cord model. *Science* 315(5817): 1416–1420.

Kafkafi N and Golani I (1998) A traveling wave of lateral movement coordinates both turning and forward walking in the ferret. *Biological Cybernetics* 78(6): 441–453.

Kalakrishnan M, Buchli J, Pastor P, Mistry M and Schaal S (2011) Learning, planning, and control for quadruped locomotion over challenging terrain. *The International Journal of Robotics Research* 30(2): 236–258.

Kelly SD and Murray RM (1995) Geometric phases and robotic locomotion. *Journal of Field Robotics* 12(6): 417–431.

Kim MS and Uther W (2003) Automatic gait optimisation for quadruped robots. In: *In Australasian Conference on Robotics and Automation*.

Kohl N and Stone P (2004) Policy gradient reinforcement learning for fast quadrupedal locomotion. In: *Proceedings IEEE International Conference on Robotics and Automation, 2004 (ICRA '04)*, Vol. 3, pp. 2619–2624.

Kolter JZ, Rodgers MP and Ng AY (2008) A control architecture for quadruped locomotion over rough terrain. In: *IEEE International Conference on Robotics and Automation, 2008 (ICRA 2008)*, pp. 811–818. IEEE.

Li C, Umbanhowar PB, Komsuoglu H, Koditschek DE and Goldman DI (2009) Sensitive dependence of the motion of a legged robot on granular media. *Proceedings of the National Academy of Sciences* 106(9): 3029–3034.

Li C, Zhang T and Goldman DI (2013) A terradynamics of legged locomotion on granular media. *Science* 339(6126): 1408–1412.

Marsden JE (1997) Geometric foundations of motion and control. In: *Motion, Control, and Geometry: Proceedings of a Symposium*. Washington, DC: Board on Mathematical Science, National Research Council Education, National Academies Press.

Marsden JE and Ratiu TS (2013) *Introduction to Mechanics and Symmetry: A Basic Exposition of Classical Mechanical Systems (Texts in Applied Mathematics*, Vol. 17). Springer Science & Business Media.

Mazouchova N, Umbanhowar PB and Goldman DI (2013) Flipper-driven terrestrial locomotion of a sea turtle-inspired robot. *Bioinspiration and Biomimetics* 8(2): 026007.

McGhee RB and Iswandhi GI (1979) Adaptive locomotion of a multilegged robot over rough terrain. *IEEE Transactions on Systems, Man, and Cybernetics* 9(4): 176–182.

McInroe B, Astley HC, Gong C, et al. (2016) Tail use improves performance on soft substrates in models of early vertebrate land locomotors. *Science* 353(6295): 154–158.

Murray RM, Li Z, Sastry SS and Sastry SS (1994) *A Mathematical Introduction to Robotic Manipulation*. Boca Raton, FL: CRC Press.

Nyakatura JA, Melo K, Horvat T, et al. (2019) Reverse-engineering the locomotion of a stem amniote. *Nature* 565(7739): 351–355.

Ostrowski J and Burdick J (1998) The geometric mechanics of undulatory robotic locomotion. *The International Journal of Robotics Research* 17(7): 683–701.

Owaki D, Kano T, Nagasawa K, Tero A and Ishiguro A (2013) Simple robot suggests physical interlimb communication is essential for quadruped walking. *Journal of The Royal Society Interface* 10(78): 0669.

Ozkan-Aydin Y, Chong B, Gong C, et al. (2017) Geometric mechanics applied to tetrapod locomotion on granular media. In: *Conference on Biomimetic and Biohybrid Systems*, pp. 595–603. Berlin: Springer.

Ozkan-Aydin Y, Rieser JM, Hubicki CM, Savoie W and Goldman DI (2019) Physics approaches to natural locomotion: Every robot is an experiment. In: *Robotic Systems and Autonomous Platforms Advances in Materials and Manufacturing*, pp. 109–127. Elsevier/Woodhead Publishing.

Palmer LR and Orin DE (2006) Attitude control of a quadruped trot while turning. In: *2006 IEEE/RSJ International Conference on Intelligent Robots and Systems*, pp. 5743–5749.

Powell MJ (1964) An efficient method for finding the minimum of a function of several variables without calculating derivatives. *The Computer Journal* 7(2): 155–162.

Qian F, Daffon K, Zhang T and Goldman DI (2013) An automated system for systematic testing of locomotion on heterogeneous granular media. In: *Proceedings of the 16th International Conference on Climbing and Walking Robots (CLAWAR)*, pp. 1–8.

Rieser JM, Gong C, Astley HC, et al. (2019) Geometric phase and dimensionality reduction in locomoting living systems. *arXiv preprint arXiv:1906.11374*.

Roos PJ (1964) Lateral bending in newt locomotion. *Proceedings of the Koninklijke Nederlandse Akademie van Wetenschappen series C - Biological and Medical Sciences* 67: 223–232.

Rossignol S, Dubuc R and Gossard JP (2006) Dynamic sensorimotor interactions in locomotion. *Physiological Reviews* 86(1): 89–154.

Saranli U, Buehler M and Koditschek DE (2001) RHex: A simple and highly mobile hexapod robot. *The International Journal of Robotics Research* 20(7): 616–631.

Schiebel PE, Astley HC, Rieser JM, et al. (2020) Mitigating memory effects during undulatory locomotion on hysteretic materials. *Elife* 9: e51412.

Shammas EA, Choset H and Rizzi AA (2007) Geometric motion planning analysis for two classes of underactuated mechanical systems. *The International Journal of Robotics Research* 26(10): 1043–1073.

Shapere A and Wilczek F (1989) Geometry of self-propulsion at low Reynolds number. *Journal of Fluid Mechanics* 198: 557–585.

Sharpe SS, Koehler SA, Kuckuk RM, et al. (2015) Locomotor benefits of being a slender and slick sand swimmer. *Journal of Experimental Biology* 218(3): 440–450.

Sprinthall RC and Fisk ST (1990) *Basic Statistical Analysis*. Englewood Cliffs, NJ: Prentice Hall.

Stone P, Dresner K, Erdogan ST, et al. (2003) UT Austin Villa 2003: A new RoboCup four-legged team. Technical Report UT-AI-TR-03-304, The University of Texas at Austin.

Suzuki S, Kano T, Ijspeert AJ and Ishiguro A (2019) Decentralized control with cross-coupled sensory feedback between body and limbs in sprawling locomotion. *Bioinspiration and Biomimetics* 14(6): 066010.

Tan J, Zhang T, Coumans E, et al. (2018) Sim-to-real: Learning agile locomotion for quadruped robots. *arXiv preprint arXiv:1804.10332*.

Wilczek F and Shapere A (1989) *Geometric Phases in Physics*, Vol. 5. Singapore: World Scientific.

Zhang T and Goldman DI (2014) The effectiveness of resistive force theory in granular locomotion. *Physics of Fluids* 26(10): 101308.

Zucker M, Ratliff N, Stolle M, et al. (2011) Optimization and learning for rough terrain legged locomotion. *The International Journal of Robotics Research* 30(2): 175–191.